PNAS
www.pnas.org

Supplementary Information for

Pervasive changes of mRNA splicing in *upf1* deficient zebrafish identify *rpl10a* as a regulator of T cell development

Divine-Fondzenyuy Lawir, Katarzyna Sikora, Connor O´Meara, Michael Schorpp, and Thomas Boehm

Corresponding author: Thomas Boehm

boehm@ie-freiburg.mpg.de

This PDF file includes:

Figures S1 to S4
SI References

Other supplementary materials for this manuscript include the following:

Datasets S1 to S6

www.pnas.org/cgi/doi/10.1073/pnas.1917812117

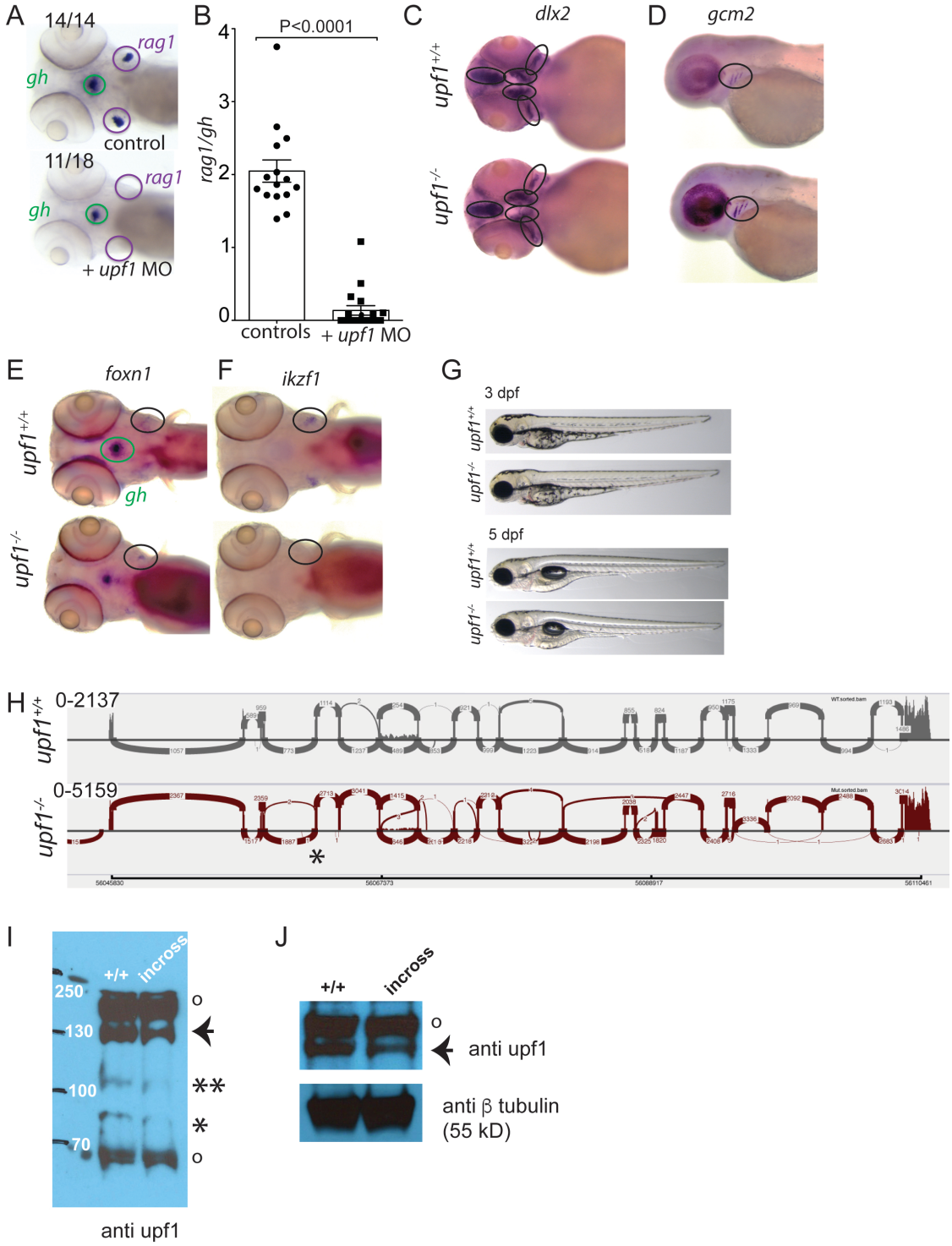

Fig. S1. Characterization of *upf1* morphants and mutants. (*A*) Phenocopy of impaired thymopoietic capacity in *upf1* morphants. Representative RNA *in situ* hybridization results are shown for *rag1* and *gh* probes. The number of embryos in each group exhibiting the WISH pattern shown is indicated; in the majority of morphants, no *rag1* signal could be detected. (*B*)

Thymopoietic capacity in *upf1* morphants. Each data point represents one fish; mean±SEM. (*C*) Representative results of RNA in situ hybridization using a neural crest-specific probe (*dlx2*). (*D*) Representative results of RNA in situ hybridization using an ectoderm-specific probe (*gcm2*). (*E*) Representative results of RNA in situ hybridization using an endoderm-specific probe (*foxn1*); the *gh* probe is used as an internal control. (*F*) Representative results of RNA in situ hybridization using a lymphocyte progenitor-specific probe (*ikzf1*). For (*C*)-(*F*), relevant expression domains are indicated. (*G*) Macroscopic appearance of *upf1* mutants and their wild-type siblings at two time points. (*H*) Sashimi plot indicating the splicing pattern of the *upf1* gene in wild-type and *upf1* mutant fish; the site of the nonsense mutation in exon 4 is indicated by *. (I) Western blot analysis of whole-embryo protein lysates of wild-type fish (+/+) and clutches generated from incross of two heterozygous parents (incross). Non-specific bands (which serve as loading controls) are indicated by “o”; the position of the full-length upf1 protein is indicated by arrow; the additional bands discussed below are marked by * and **, respectively. In protein lysates of pooled embryos from a cross of two heterozygous parents, only 50% of the normal amount of protein is seen, as expected. A proportional reduction is also seen for two smaller proteins, of ~110kD (**) and ~90kD (*); hence, we consider these fragments to be degradation products. However, the ~90kD fragment may also arise from use of an internal translational start site located downstream of the premature stop codon in the mutant *upf1* transcript. (J) Western blot analysis, similar to panel (I); in this experiment, the filters were sequentially probed with antibodies raised against upf1 and β-tubulin, the latter protein serving as loading control.

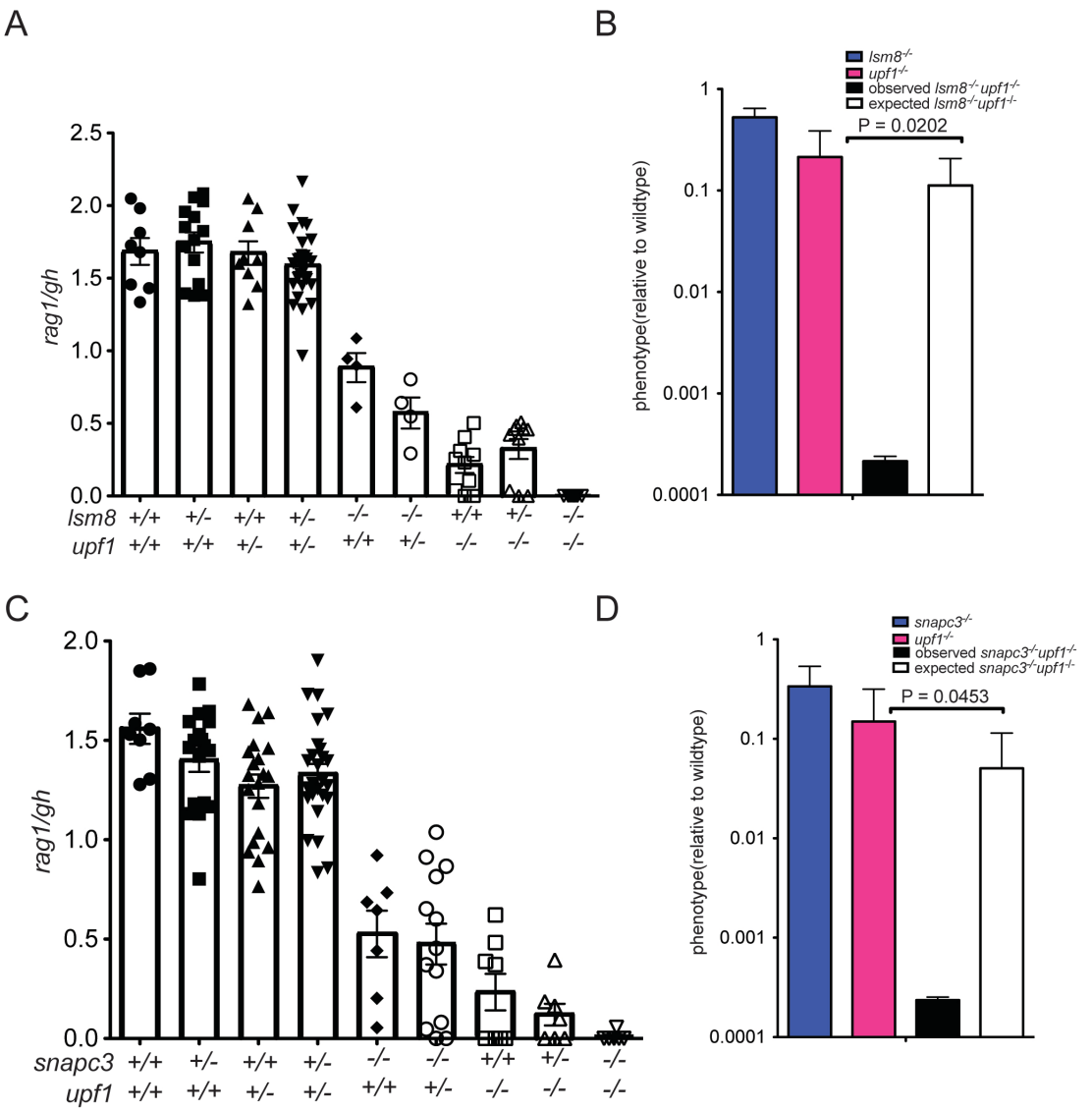

Fig. S2. Epistasis analysis of the *upf1* mutation. (*A*) Thymopoietic capacities measured in fish of the nine genotypes arising from an intercross of *upf1*$^{+/-}$;*lsm8*$^{+/-}$ double-heterozygous parents (each data point represents one fish; mean±SEM). (*B*) Comparison of phenotypes of the two single mutants (*upf1*$^{-/-}$ and *lsm8*$^{-/-}$, respectively), and the *upf1*$^{-/-}$;*lsm8*$^{-/-}$ double mutant; the latter phenotype is compared to the expected phenotype (multiplicative model). The thymopoietic capacity observed in the double mutant is significantly lower than expected from the combination of the single mutants, calculated under the assumption of no genetic interaction, indicative of synthetic genetic interaction. (*C*) Thymopoietic capacities measured in fish of the nine genotypes arising from an intercross of *upf1*$^{+/-}$;*snapc3*$^{+/-}$ double-heterozygous parents (each data point represents one fish; mean±SEM). (*D*) Comparison of phenotypes of the two single mutants (*upf1*$^{-/-}$ and *snapc3*$^{-/-}$, respectively), and the *upf1*$^{-/-}$;*snapc3*$^{-/-}$ double mutant; the latter phenotype is compared to the expected phenotype (multiplicative model). The thymopoietic capacity observed in the double mutant is significantly lower than expected from the combination of the single mutants, calculated under the assumption of no genetic interaction, indicative of synthetic genetic interaction.

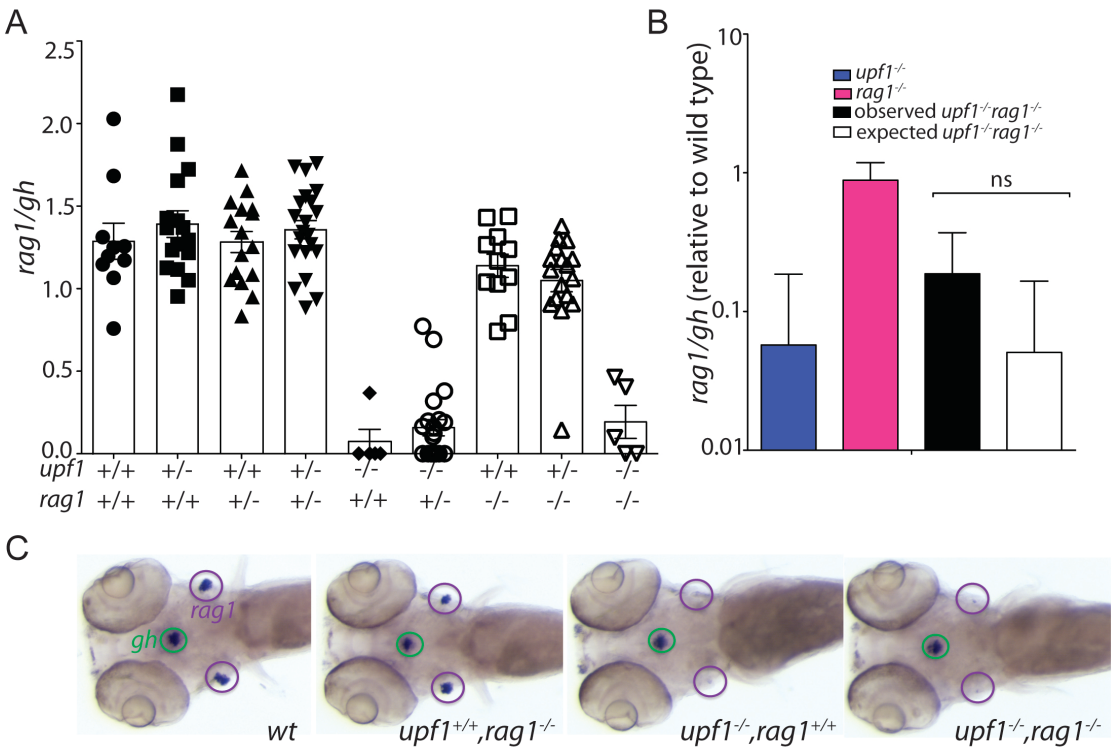

Fig. S3. Epistasis analysis of the *upf1* mutation. (*A*) Thymopoietic capacities measured in fish of the nine genotypes arising from an intercross of *upf1*$^{+/-}$;*rag1*$^{+/-}$ double-heterozygous parents (each data point represents one fish; mean±SEM). Representative whole-mount RNA *in situ* hybridization results for the key genotypes are shown at the bottom of the panel. (*B*) Comparison of phenotypes of the two single mutants (*upf1*$^{-/-}$ and *rag1*$^{-/-}$, respectively), and the *upf1*$^{-/-}$;*rag1*$^{-/-}$ double mutant; the latter phenotype is compared to the expected phenotype (multiplicative model). The thymopoietic capacity observed in the double mutant is in the range expected from the combination of the single mutants, calculated under the assumption of no genetic interaction, indicative of lack of genetic interaction.

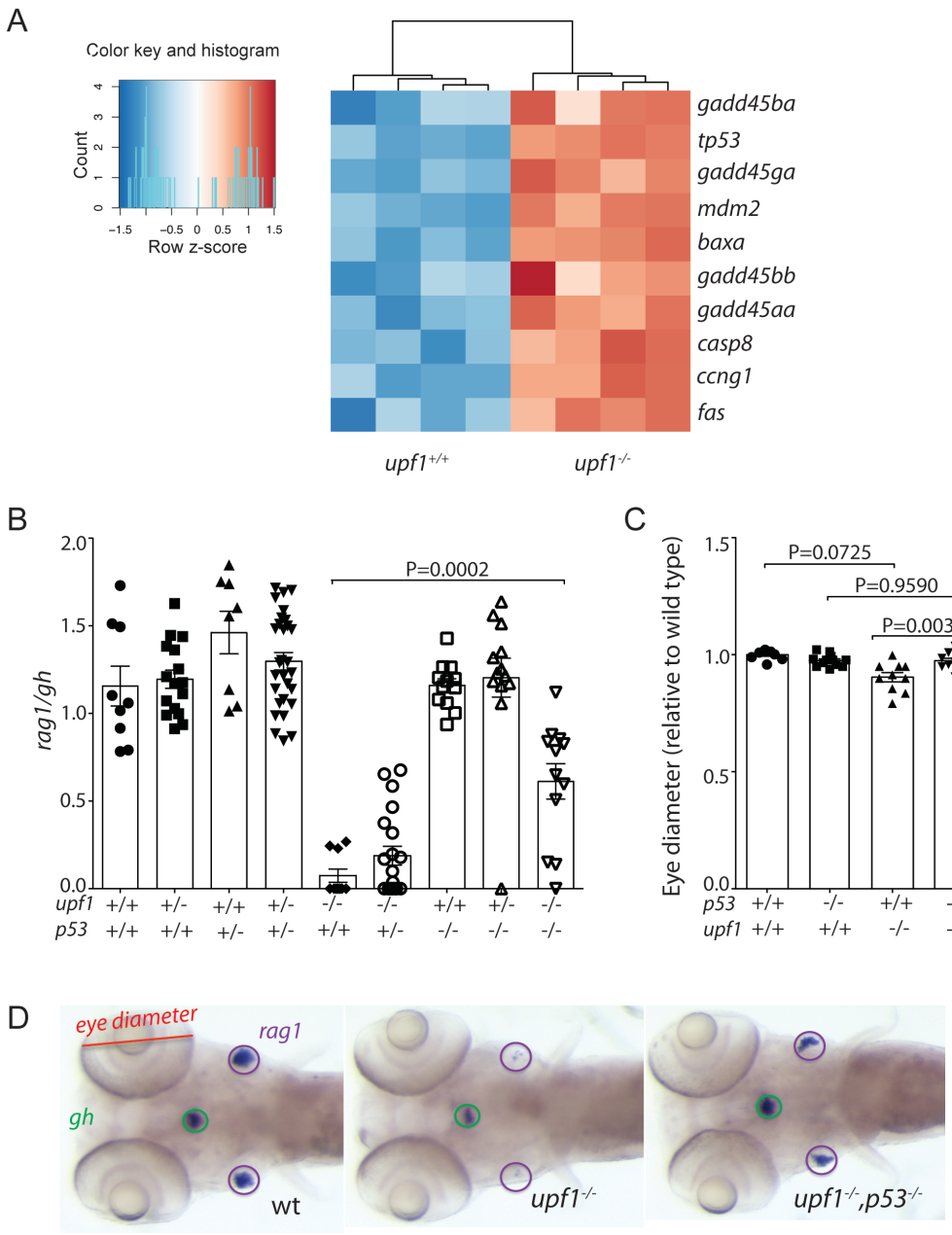

Fig. S4. Epistasis analysis of the *upf1* mutation. (A) Up-regulation of genes in the p53 signaling pathway in *upf1* mutants. Gene-level quantification was used. (*B*) Thymopoietic capacities measured in fish of the nine genotypes arising from an intercross of *upf1*$^{+/-}$;*p53*$^{+/-}$ double-heterozygous parents (each data point represents one fish; mean±SEM). Note that the thymopoietic index of the double mutant is significantly higher than that of the *upf1* single-mutant. (*C*) Comparison of phenotypes of the two single mutants (*upf1*$^{-/-}$ and *p53*$^{-/-}$, respectively), and the *upf1*$^{-/-}$;*p53*$^{-/-}$ double mutant; the latter phenotype is compared to the expected phenotype (multiplicative model). The size of the eye (largely determined by neuronal structures) observed in the double mutant is significantly higher than expected from the combination of the single mutants, calculated under the assumption of no genetic interaction, indicative of positive (alleviating) genetic interaction. (*D*) Representative whole-mount RNA *in situ* hybridization results for the key genotypes in (*B*).

Dataset S1 (separate file). List of genes in the zebafish genome giving rise to NMD-susceptible transcripts.

Dataset S2 (separate file). Altered expression levels of NMD-susceptible transcripts in *upf1* mutants.

Dataset S3 (separate file). Altered expression levels of non-NMD transcripts in *upf1* mutants.

Dataset S4 (separate file). Intersect of dysregulated genes between zebrafish *upf1* and mouse *upf2* mutants

Dataset S5 (separate file). Intersect of dysregulated genes between zebrafish *upf1* and mouse *upf2* mutants (1).

Dataset S6 (separate file). Altered expression levels of non-NMD transcripts in *tnpo3* mutants.

SI Reference

1. J. Weischenfeldt, et al. (2012) Mammalian tissues defective in nonsense-mediated mRNA decay display highly aberrant splicing patterns. *Genome Biol* 13, R35 (2012).